Journal of
Water & Climate Change

© 2024 The Authors Journal of Water and Climate Change Vol 15 No 6, 2648 doi: 10.2166/wcc.2024.632

Application of artificial countermeasures to enhance desilting efficiency in a reservoir under normal and extreme events

Fong-Zuo Lee * and Nhat Lam Huynh Nguyen

Department of Civil Engineering, National Chung Hsing University, 145 Xingda Rd., South Dist., Taichung City 402202, Taiwan (R.O.C.)
*Corresponding author. E-mail: fzlee@nchu.edu.tw

F-ZL, 0000-0003-0826-1435

ABSTRACT

The influx of flood-induced turbidity flows with high sediment concentrations into the reservoir can create sediment deposition issues, potentially jeopardizing water supply reliability. Efficient management of reservoir water resources is imperative for sustainable utilization. Evaluating the need for reservoir desilting involves comprehending the inflow and outflow dynamics of water-sediment discharges, the capacity of existing outlet structures, reservoir operation objectives, and available desilting technologies. However, given the altering hydrological conditions due to the impacts of climate change, there is a necessity for adaptive methods to ensure reservoir storage maintenance. Consequently, this study introduces the utilization of a flushing channel with artificial guiding structures to enhance desilting efficiency. A 2D numerical model offers convenient computational tools for assessing water-sediment transport behaviors across various operational scenarios based on reservoir management strategies. Data obtained from field observations is collected and analyzed to calibrate and verify the numerical model. By employing 2D numerical modeling, sediment concentration and desilting efficiency are calculated to support effective desilting operations within a reservoir. Simulation results indicate that the integration of additional artificial guiding structures at the bottom of the reservoir can enhance sedimentation mitigation outcomes by approximately 17.63% under normal conditions and by 5.27% under extreme hydrological conditions.

Key words: adaptive methods, artificial guiding structures, desilting efficiency, sediment deposition

HIGHLIGHTS

- A typical method is to prevent sediment movement toward the dam. We propose a new concept to partially guide and concentrate inflow sediment using artificial structures toward the outlet. This concept has not been proposed or discussed before.
- We present the contribution of adapted artificial countermeasures under different hydrological conditions that can provide a reference strategy for worldwide reservoir management.

1. INTRODUCTION

The construction of dams typically involves planning for a life expectancy of 100 years, providing ample dead storage capacity to sustain functionality over this period through the gradual accumulation of sediments (Wieland 2010). Despite this foresight, reservoir deposition, a sedimentation process, poses a significant challenge to both storage capacity and flood control ability. Reservoir sedimentation emerges as a crucial issue in dam construction, leading to a gradual reduction in the active storage of global reservoirs each year. This decline has prompted a growing necessity for building new reservoirs, contributing to an ongoing loss of storage space. It is reported that the loss in the reservoir storage capacity worldwide ranges from 0.5 to 1% per annum (Wisser *et al.* 2013). In the Asian region, the loss in the reservoir storage capacity rises to 2.9% (WRA 2020a). Reservoir sedimentation is caused by the gradual deposition of an incoming sediment load from its catchment. The issue of reservoir sedimentation has caused significant problems in many parts of the world, resulting in severe implications for water conservation, flood control, and energy production. The sediment settling phenomenon in the reservoir is influenced by various factors, including the hydrology of the catchments and the characteristics of the river basin. A humongous structure like a dam, even though highly beneficial, eventually becomes a cause of problems in our naturally balanced river ecosystem. Sediment inflow and outflow are naturally balanced in the streams with no obstruction. Structures like dams disturb this naturally developed balance. As the sediment-laden flow reaches the reservoir, its velocity decreases as it approaches the dam body. This decrease in the velocity causes the settling of the suspended sediments destined to flow downstream in the suspended state only. Reservoir sedimentation has been a problem for a very long time, but it received little to no attention in the early 20th century. Unfortunately, no single permanent solution was developed to tackle the problem of reservoir sedimentation during the dam's operation period. It is neither cost-effective nor environmentally sustainable to demolish the existing dam to restore the reservoir's storage capacity and sediment balance. Thus, a responsibility lies on the shoulders of the researchers to develop better and more effective management techniques so that there is enough reservoir storage to fight the problems of heavy flooding and drought. With the unusual climate change, the frequency of floods and droughts is likely to increase in the future. Thus, it has become essential to develop a technique to mitigate the problem of reservoir sedimentation and ensure the sustainability of reservoirs.

The migration of high-concentration sediment to the front of the dam can cause the interruption of water supply and the reduction of water storage (Morris & Fan 2010); reservoir siltation is a persistent water resource problem. To maintain reservoir capacity and stabilize water supply, it is necessary to develop sediment management and desilting countermeasures to ensure sustainable operation of the reservoir (Kondolf *et al.* 2014); reservoir desilting strategies can be divided into four aspects: catchment area conservation, reservoir dredging and deposition reduction, reservoir storage capacity restoration, and adaptive strategies (Annandale *et al.* 2016; WRA 2020a). However, the planning of reservoir sediment management strategies needs to be multi-adapted or improvement to local conditions. Various strategies are employed to manage sediment flow into reservoir zones. One common approach involves the construction of check dams upstream of the reservoir, aiming to reduce sediment inflow and maintain storage capacity (Samad *et al.* 2016; Zeng *et al.* 2022; Zulfan *et al.* 2023). However, inflow sediment with fine sediment will eventually be transported to the dam site due to the limited capacity of upstream prevention strategies. Dredging is another method utilized to excavate sediment from the reservoir at regular intervals, excluding typhoon periods, effectively extending the reservoir's lifespan (Smith *et al.* 2013; Ge *et al.* 2021; Kantoush *et al.* 2021). In addition, the implementation of a bypass tunnel is considered an effective sediment release strategy, particularly during typhoons. This approach allows sediment to be directed through the tunnel to the downstream river, preventing sediment deposition on the reservoir bed (Albayrak *et al.* 2019; Boes *et al.* 2019; Morris 2020). Various improvement techniques of artificial countermeasures are also under study to impede sediment flow into the reservoir. The definition of artificial countermeasure methods involves utilizing man-made structures, also referred to as artificial guiding structures, to enhance desilting efficiency. Examples include solid obstacles and permeable obstacles at the reservoir bottom (De Cesare *et al.* 2006; Oehy & Schleiss 2007; Baghalian & Ghodsian 2020), aiming to enhance the desiltation effect of the reservoir. However, the flushing channel, when left empty, demonstrates relatively better desilting efficiency (Chen & Tsai 2017; Wang *et al.* 2020; WRA 2020a). The application of the main channel characteristic concept to the flushing channel is also employed during high-water-level conditions (Chen 2022). Nevertheless, the location and configuration of the flushing channel change with the hydrological and hydraulic characteristics of inflow and outflow (Lai & Shen 1996; Wang *et al.* 2020). To mitigate uncertainty and facilitate maintenance, this study introduces an innovative concept. It involves utilizing artificial guiding structures within the flushing channel to enhance desilting efficiency. The concept is to concentrate and accelerate the movement of turbid inflow water towards the outlet. It is theoretical to increase desilting efficiency and prevent sediment deposition on the reservoir bottom.

A numerical model is generally considered a promising and effective tool for reservoir desiltation study. The 2D numerical model seems to be a suitable model for studying such turbidity current inflow in the field reservoir because of the advantages of the simulation efficiency from the 1D model and the accuracy from the 3D model (Lai 2010). However, the 2D model may not be suitable for the case of simulation of sediment transportation in reservoirs due to its deep-water condition without equation modification or considering the reservoir characteristics. This means that the reservoir characteristics, including geometry, operation, and desilting strategies, will dominate numerical model performance and applicability. Therefore, we collect relevant studies of the 2D model to realize its applicability. Hu *et al.* (2012) adopted the 2D turbidity current model to investigate the turbidity current transport rate in the site reservoir. The results indicated that it could be a valuable tool for operating the sluice gates to release excess sediment from the reservoir. Huang *et al.* (2019) found that the 2D model is capable of predicting the movement of turbidity current toward the dam site and the sluicing out of outlets at different elevations and is valid to practice for field applications. The study also established guidelines for suitable sensitivity parameter ranges in the field site and presented that the mesh size and drag coefficient are crucial parameters that need to be considered.

Anari *et al.* (2020) indicated that the 2D model is appropriate for simulating the horizontal movement of the turbidity current, especially the release behavior near the reservoir sluice gates. The most important is that considering sediment transportation in reservoir management is crucial for ensuring reservoir storage sustainability. The 2D model research related to the establishment of a desilting channel at the bottom of the Zengwen Reservoir including bottom dredged channels was adapted to simulate the sediment concentration and desilting efficiency (Chen 2020). Wang *et al.* (2020) proposed a strategy through 2D model simulations that involves compartmentalizing the reservoir. This strategy has shown significant enhancements in terms of flushing efficiency. The degree of improvement varies based on specific scenarios, encompassing partition desilting, empty flushing, or a hybrid approach that combines both methods. In addition, the studies of Chen and Tsai (2017) and Wang *et al.* (2020) indicate that creating a narrower gorge-like geometry is helpful to increase desilting efficiency. A 2D numerical model can also be used to simulate the weir area to explore the effect of different types of hydraulic structures on flood control and deposition reduction (Lee *et al.* 2021). Hung *et al.* (2022) used a 2D turbidity currents model to simulate the movement of turbidity currents and the distribution of sediment concentration in the Shihmen Reservoir area; the outflow discharge and concentration processes of the desilting facilities were also investigated. Regarding the improvement technique to enhance the reservoir desiltation efficiency, apart from the field implementation and physical model test, the numerical model is technically regarded as a consistent and practical analysis approach for turbidity current flow. Lee *et al.* (2023a, 2023b) studied a main flushing channel in the current terrain of the Agongdian Reservoir using a 2D numerical model to set up and analyze the impact of the sedimentation mitigating using steady-state conditions. Therefore, an appropriate 2D numerical model is valuable and acceptable to study a flushing channel with artificial guiding structures to enhance desilting efficiency in a reservoir.

2. METHODS

2.1. Study site information

Located in Southern Taiwan, the Agongdian Reservoir encompasses a drainage area of 29.6 km^2. It serves as a versatile reservoir primarily designed for flood control, safeguarding the Yanchao area against flood levels projected for a 250-year flood. The reservoir, situated at the confluence of the Wanglai and Zhoushui Rivers, offers additional functions beyond flood regulation. In addition to flood control, the reservoir is effectively utilized for irrigation, recreation, and meeting municipal and industrial water needs. Its geographical layout involves the northern and southeast inlets of the Wanglai and Zhoushui Rivers situated on opposing sides (Figure 1). Structurally, the Agongdian Reservoir comprises a dam, a morning glory spillway, and an intake tower. Two outlets, namely, the spill shaft and the irrigation shaft, are positioned near the dam face. These outlets play a crucial role in diverting both water and sediment out of the reservoir, contributing to its overall management and functionality.

Within the Yanchao District of Kaohsiung City, Taiwan, stands the dam of the Agongdian Reservoir, erected in 1953 and measuring 31 m in height. Regrettably, the reservoir's potential to attain full capacity is hindered by the accumulation of sediment. With a broad, short, and shallow configuration, the Agongdian Reservoir was initially designed with a maximum water level set at an elevation of 40 m, equating to a comprehensive storage capability of 36.7 million m^3. Yet, as of 2022, the impact of sedimentation has been significant. The reservoir has suffered a loss of more than 41.41% of its initial storage capacity (WRA 2022a). This depletion leaves the reservoir with a mere 15.2 million m^3 of storage capacity. Notably, an additional gauging station is positioned at the reservoir's spill shaft, enhancing its monitoring and management.

The primary cause for concern regarding sediment management at the Agongdian Reservoir is the rapid rate of sedimentation (WRA 2020b). This swifter sedimentation is primarily attributed to the substantial sediment yield from the reservoir's southeast tributary, the Zhoushui River, which carries two to three times more sediment than the northern tributary, the Wanglai River (WRA 2020b). The Zhoushui River is further characterized by a steeper slope and a narrower channel than the Wanglai River. Consequently, this results in a heightened inflow velocity and the creation of an erosion channel at its inlet (Chen & Tsai 2017). However, due to the current reservoir configuration, this erosion channel dissipates within the reservoir without evolving into a continuous flushing channel.

Between 1997 and 2003, an assortment of physical and numerical experiments was conducted to aid the development of sediment management strategies aimed at revitalizing the storage capacity of the Agongdian Reservoir (WRA 2003). The culmination of these experiments contributed to the formulation of an engineering design. The outcomes of the physical experiments highlighted the potential enhancement of sediment release efficiency to 65.3%. This transformation hinged

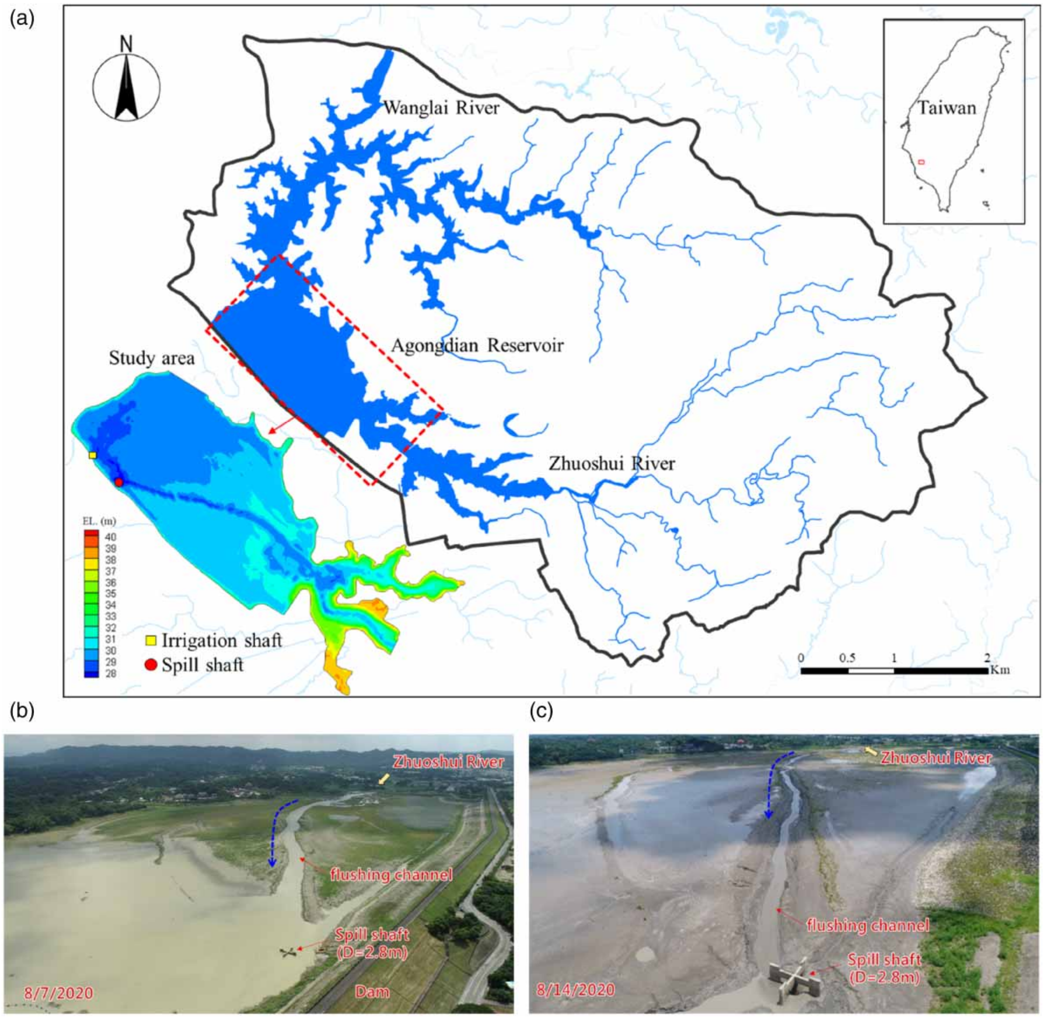

Figure 1 | Study site. (a) Reservoir location and study area information; (b, c) field pictures of the flushing channel.

upon the adjustment of the spillway's opening, coupled with an enlargement of the internal diameter of the spillway (WRA 2003). With these findings as a foundation, a multi-phase renovation initiative was set into motion and carried out until 2006. One pivotal aspect of these renovations involved the reduction of the sluice gate's height on the spill shaft. This modification aimed at augmenting the outflow discharge and sediment concentration. Following the comprehensive implementation of the renovation project, not only did the Agongdian Reservoir's flood protection capacity extend to a 10,000-year flood event, but it also succeeded in reinstating the storage capacity to 18.4 million m^3 by 2006. The implications of this achievement are noteworthy. For 53 years, the reservoir's storage capacity dwindled from an initial 36.7 to 18.4 million m^3, equating to a deposition rate of around 0.35 million m^3 annually. However, following the completion of the renovation project, the deposition rate witnessed a decline to 0.20 million m^3 per year during the period spanning from 2006 to 2022.

The intended benefits of the renovation project have encountered limitations stemming from diverse pressures, including the desire to maintain a scenic waterscape for tourism and concerns regarding downstream safety. These pressures have led to alterations in the reservoir's operational approach, impeding the primary objective of enhancing desilting efficiency. Consequently, the existing water storage operation is curtailed during non-typhoon periods. In addition, when confronted with typhoons or heavy rainfall, the maximum allowable outflow discharge is restricted to 90 m^3/s to mitigate downstream flooding. In light of these challenges, a novel concept for improvement has been introduced. This concept aims to bolster desilting efficiency even within the constraints of such operational conditions.

Since the 2006 renovation and improvement, a flushing channel gradually emerged in the middle of the reservoir, formed by the scouring action of the Zhuoshui River. Starting in 2019, the Water Resources Agency (WRA) expanded and excavated this artificial deep channel along the gully to facilitate sediment flushing. However, due to varying hydrological conditions and reservoir flood and sediment prevention operations, the position, depth, and geometric shape of the flushing channel may change. Therefore, if artificial guiding structures, such as steel sheet piles along both sides of the main channel, can be employed to stabilize its form, it would be beneficial for maintenance and quantifying the effectiveness of sediment prevention. Consequently, the concept of applying steel sheet piles to enhance desilting efficiency is introduced in this study. This study is initiated for this reason and initially adopts a flushing channel with a width of 15 m, height of 1.5 m, and a slope of approximately 1/300 based on the current situation for further exploration. The location, length, and height of steel sheet piles are listed in Figure 2 and Section 2.4.

2.2. Numerical methodology

2D models hold significant value for reservoir and water managers due to their capacity to account for intricate topographies and flow characteristics. The Sedimentation and River Hydraulics (SRH-2D) model, a numerical tool adept at portraying two-dimensional hydraulic and sediment transport phenomena, has proven its utility in this domain (Huang *et al.* 2019; Wang *et al.* 2020). The model's capabilities extend to the simulation of various flow conditions, encompassing steady, quasi-steady, and unsteady flows. Furthermore, it accommodates both cohesive and non-cohesive states for sediment transport.

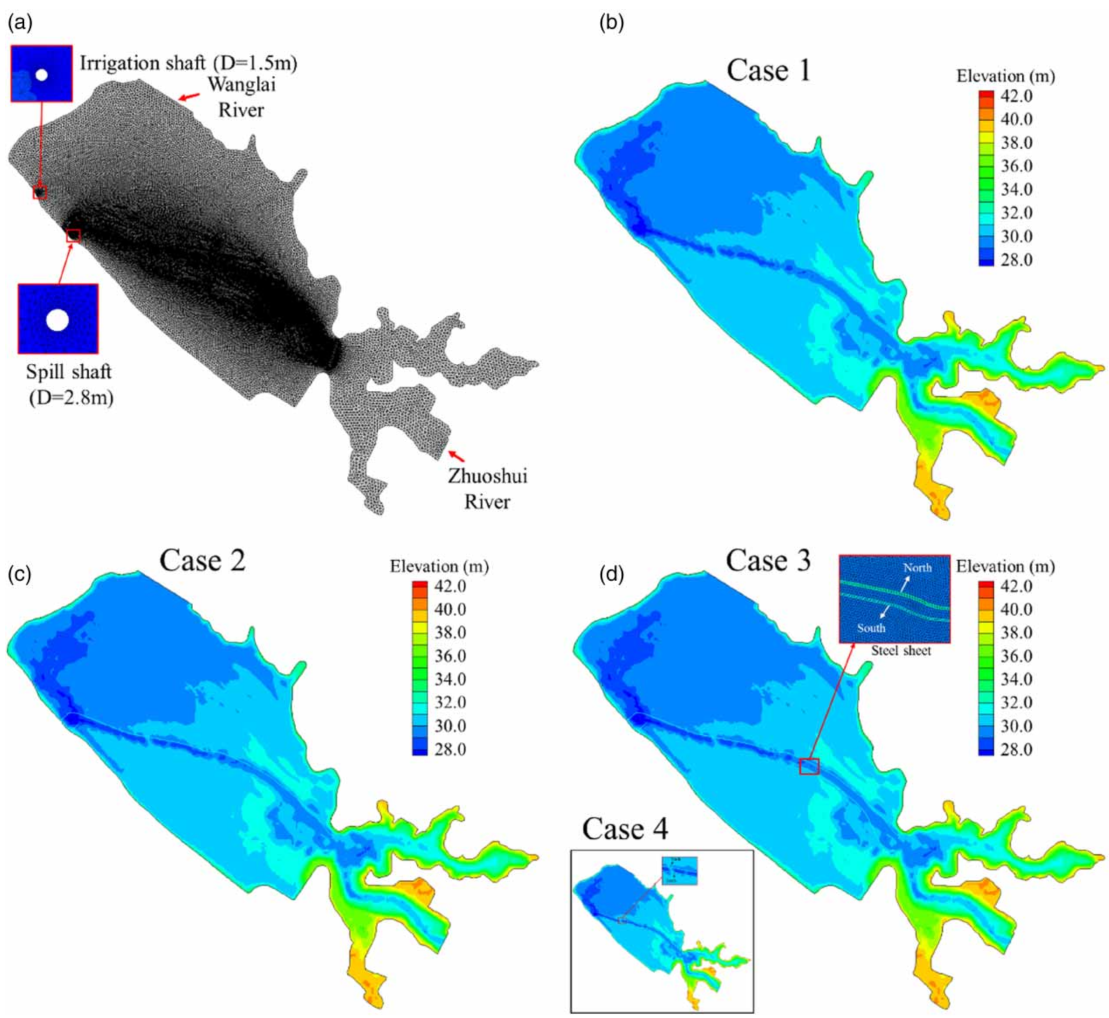

Figure 2 | Simulation. (a) Grids; (b) elevation without steel sheet piles; (c) elevation with north steel sheet piles; (d) elevation with north and south steel sheet piles.

Notably, the model offers the flexibility to opt for multi-size sediment transport, incorporating features like bed sorting and armoring (Lai 2010). This comprehensive functionality enables the SRH-2D model to be an indispensable tool in assessing diverse scenarios of sediment transport and hydraulic behavior. The SRH-2D model exhibits the capability to anticipate alterations in the bed profile through the tracking of non-equilibrium sediment transport. This encompasses scenarios involving suspended, mixed, and bed loads on various types of beds including granular, erodible rock, or non-erodible substrates, in addition to accounting for bank erosion (Lai 2020). For most open channel flows, their shallowness renders vertical motions negligible in terms of their impact. Consequently, the three-dimensional Navier–Stokes equations can be averaged vertically to yield a set of depth-averaged 2D equations, which subsequently gives rise to the standard St. Venant equations. The model employs these equations, rooted in mass conservation and momentum principles, to solve the underlying hydraulic mechanisms, as depicted in Equations (1)–(3):

$$\frac{\partial h}{\partial t}+\frac{\partial hU}{\partial x}+\frac{\partial hV}{\partial y}=0, \tag{1}$$

$$\frac{\partial hU}{\partial t}+\frac{\partial hUU}{\partial x}+\frac{\partial hVU}{\partial y}=\frac{\partial hT_{xx}}{\partial x}+\frac{\partial hT_{xy}}{\partial y}-gh\frac{\partial z}{\partial x}-\frac{\tau_{bx}}{\rho}, \tag{2}$$

$$\frac{\partial hV}{\partial t}+\frac{\partial hUV}{\partial x}+\frac{\partial hVV}{\partial y}=\frac{\partial hT_{xy}}{\partial x}+\frac{\partial hT_{yy}}{\partial y}-gh\frac{\partial z}{\partial y}-\frac{\tau_{by}}{\rho}, \tag{3}$$

where h is the water depth; t is the time; U and V are the depth-averaged velocity components in x and y directions, respectively; x and y are the horizontal Cartesian coordinates; T_{xx}, T_{xy}, and T_{yy} are the depth-averaged stresses due to turbulence and dispersion; g is the gravitational acceleration; $z = z_b + h$ is the water surface elevation; z_b is the bed elevation; τ_{bx} and τ_{by} are the total bed shear stresses; and ρ is the water density.

For sediment transport, each sediment size in the water column is governed by the following non-equilibrium mass conservation Equation (4):

$$\begin{aligned}&\frac{\partial hC_k}{\partial t}+\frac{\partial \cos(\alpha_k)\beta_k V_t hC_k}{\partial x}+\frac{\partial \sin(\alpha_k)\beta_k V_t hC_k}{\partial y}\\&=\frac{\partial}{\partial x}\left(hf_kD_x\frac{\partial C_k}{\partial x}\right)+\frac{\partial}{\partial y}\left(hf_kD_y\frac{\partial C_k}{\partial y}\right)+S_{e,k}.\end{aligned} \tag{4}$$

In the above equation, C_k is the depth-averaged sediment concentration by volume and subscript k denotes that the variable is for sediment size class k, α_k is the angle of the sediment transport direction relative to the x-axis, β_k is the sediment-to-flow velocity ratio, $V_t=\sqrt{U^2+V^2}$ is the depth-averaged flow velocity, f_k is the transport mode parameter representing the suspended load fraction, D_x and D_y are the sediment mixing coefficients in the x and y directions, respectively, and $S_{e,k}$ is the sediment exchange rate between sediments in the water column and those in the active layer or on the bed.

Bed elevation changes are a cumulative result influenced by sediment size classes. These changes are calculated by assessing the net sediment exchanges between particles in the water column and those within the active layer. The change in z_b due to sediment size class k obeys the following equation:

$$\eta_{a,k}\left(\frac{\partial z_b}{\partial t}\right)_k=-\dot{V}_k=-\frac{q^*_{t,k}-\beta_k V_t hC_k}{L_{b,k}}, \tag{5}$$

where $\eta_{a,k}=1-\sigma_{a,k}$ is the porosity parameter of the active layer, $\sigma_{a,k}$ is the porosity for sediment size class k in the active layer, $\dot{V}_k$ is the net volumetric rate of erosion per unit area (or net rate of eroded depth) for size class k, $q^*_{t,k}$ is the total load transport capacity for sediment size class k, and $L_{b,k}$ is the bed load adaptation length for sediment size class k. The above equation provides the net erosion and deposition of the sediments, which would alter the sediment contents in the active layer. The above detailed descriptions of governing equations from Equations (1)–(5) can be found in Lai (2020).

2.3. Initial and boundary conditions

This study involved the utilization of the SRH-2D model, necessitating the provision of boundary, surface, and bottom conditions as identified and calculated in the preceding phase. For the upstream boundary conditions, hourly discharge hydrographs were utilized. These hydrographs integrated regressed sediment discharge information collected from two key gauging stations. The Bailing Culvert station is situated along the Zhuoshui River, and the Doulao Temple station is situated along the Wanglai River (Wang *et al.* 2020). In contrast, the downstream boundary was defined using discharge hydrographs extracted from the spill shaft and the irrigation shaft. As in the WRA (2015) investigation, landslides from the upstream catchment emerged as the primary sediment source for the reservoir. Consequently, it was deduced that sediment inflow from the downstream catchment could be reasonably disregarded. To devise an effective predictive approach for the field site, this study diligently assembled four comprehensive sets of time-series field data. These encompassed the hydrological records for inflow and outflow alongside sediment-related data. The amalgamation of these data sets played a pivotal role in the formulation of a valuable predictive framework tailored to the conditions of the site.

Moreover, pertinent data to be input into the two-dimensional model included a mesh network generated from contour maps, data on bottom roughness, and the median size of sediment diameters. Of paramount importance is the calibration of parameter settings, as it plays a pivotal role in ensuring the accuracy of simulations conducted at the field site. To suit the numerical model's requirement of representing the reservoir's topography with cells and nodes, the Surface Water Modeling System software was employed. This software, utilizing contour maps as its foundation, was responsible for generating boundaries, meshes, and defining areas of bottom roughness. To commence this process, contour maps were initially constructed by incorporating the data obtained from topography surveys conducted at the year end. These maps portrayed the reservoir impoundment's topography before the occurrence of any typhoons during that specific year. The employed topographic survey data were systematically conducted within an expansive 145-ha area characterized by a water surface elevation of 40 m. To meet the computational demands, a suggested mesh number exceeding 4,000 (Huang *et al.* 2019) was adopted. In this study, a substantial 104,615 mesh configuration was employed, featuring a cell size spanning from 2 to 15 m to facilitate the simulation procedures. The calibration of Manning's roughness coefficient, fundamental to modeling the reservoir, involved a comparison between computed and observed water surface profiles.

Drawing inspiration from Wang *et al.* (2020), a Manning roughness coefficient of 0.020 was adopted in accordance with their recommendations. Complementing these coefficients, data regarding bottom roughness was included. In addition, a consistent median sediment diameter size of approximately 0.039 mm was gathered for the entire impoundment area, drawing from the findings of Lee *et al.* (2023a).

The execution of the SRH-2D model encompassed two distinct steps: first, the initiation of a flow routine model; subsequently, the implementation of a mobile-bed model to facilitate the generation of concentration plots based on specific hydrological circumstances. The simulation's temporal intricacies were calibrated, with a time step set at 1 s and a result output frequency established at 1 h. In terms of the turbulence model, a parabolic model was embraced, while sediment-specific parameters were also outlined. The density for sediment was defined at 2,700 kg/m^3, while the sediment transport capacity equation adhered to Parker's (1990) formulation.

2.4. Study cases

Based on field measurement data in the last decade, the historical typhoon events and valued data collection are selected for numerical model verification (Wang *et al.* 2020). According to the parameters referenced and the model simulation settings mentioned in Section 2.2, Typhoons Fanapi, Talim, Megi, and Nesat were chosen for model calibration and verification. The basic hydrological condition is presented as listed in Table 1.

After model calibration and verification, two application scenarios using a flushing channel with artificial guiding structures are presented to investigate the desilting efficiency and sediment transportation in the Agongdian Reservoir. By complementing artificial guiding structures, such as steel sheet piles along both sides of the main channel, it is possible to control and maintain the turbid inflow mechanism of the Zhuoshui River. In addition to expecting to achieve high-concentration sediment collection and increase desilting efficiency using artificial guiding structures, there is also the benefit of reducing sediment deposition in the reservoir. This approach is also advantageous for annual maintenance and mechanical dredging operations. Consequently, the concept of applying steel sheet piles to enhance desilting efficiency is introduced in this study. The location, length, and height of steel sheet piles are listed in Figure 2 and Table 2.

Table 1 | Model calibration and verification cases

Typhoon events	Zhuoshui River peak flow rate (m^3/s)	Wanglai River peak flow rate (m^3/s)	Initial water level (m)	Return period
Typhoon Fanapi	73.56	32.84	31.64	<Q1.11
Typhoon Talim	64.51	25.14	30.45	<Q1.11
Typhoon Megi	174.76	213.60	34.53	Q5–Q10
Typhoon Nesat	125.46	153.34	30.28	Q2–Q5

Table 2 | Research scenarios

Cases	Artificial guiding structures (length and elevation)	Zhuoshui River peak flow rate (m^3/s)	Wanglai River peak flow rate (m^3/s)	Initial water level (m)	Return period	Events
Case1-1	–	47	81	28	Q1.11	Normal
Case1-2		47	81	30	Q1.11	Normal
Case1-3		161	278	28	Q10	Medium
Case1-4		363	627	28	Q1000	Extreme
Case2-1	North (length is 1,387.2 m with EL. 32 m)	47	81	28	Q1.11	Normal
Case2-2		47	81	30	Q1.11	Normal
Case2-3		161	278	28	Q10	Medium
Case2-4		363	627	28	Q1000	Extreme
Case3-1	North (length is 1,387.2 m with EL. 32 m) South (length is 656.9 m with EL. 32 m and length is 710.3 m with EL. 30 m)	47	81	28	Q1.11	Normal
Case3-2		47	81	30	Q1.11	Normal
Case3-3		161	278	28	Q10	Medium
Case3-4		363	627	28	Q1000	Extreme
Case3-5		88	152	28	Q2	Normal
Case3-6		131	227	28	Q5	Medium
Case3-7		200	345	28	Q25	Severe
Case3-8		229	396	28	Q50	Severe
Case3-9		290	500	28	Q200	Extreme
Case4-1	North (length is 1387.2 m with EL. 32 m) South (length is 656.9 m with EL. 32 m and length is 710.3 m with EL. 32 m)	47	81	28	Q1.11	Normal
Case4-2		47	81	30	Q1.11	Normal
Case4-3		161	278	28	Q10	Medium
Case4-4		363	627	28	Q1000	Extreme

To ensure the robustness of the simulation model across various scenarios, additional return period scenarios were incorporated, as listed in Table 2. These scenarios ranged across different disaster scales, namely, slight, medium, and extreme and were introduced to assess the model's consistency. In addition, the normal, medium, severe, and extreme classifications between the Q1.11 and Q1000 return periods are distinguished to study the desilting effect change. Based on the main inflow sediment coming from the Zhuoshui River, one improvement concept, Case 2, is to construct steel sheet piles at the north part of the existing flushing channel to prevent sediment transportation into the relatively clear water area. The second improvement concept, Case 3, considers a narrow and constrained channel using steel sheet piles at both sides of the existing flushing channel to concentrate sediment transportation and expects to increase the desilting efficiency of the spill shaft. However, based on the engineering costs, constructability, safety, and operational maintenance concerns, different heights of steel shafts on the southern side from upstream to downstream were adapted for this study (WRA 2022b). The downstream part of the south steel sheet piles is designed at a lower elevation to guide overflow discharge mainly toward the Southern part of the reservoir.

In addition, we have added Case 4 condition of uniform-height steel shafts between the northern and southern parts to further discuss the desilting performance. The topographic condition in 2022 is adapted as a background for four cases. The design simulation cases and their related topographic terrain are listed and shown in Table 2 and Figure 2. In addition, the design hydrograph of 29 h is adapted for the unsteady simulation, and the inflow sediment load is regressed using inflow discharge (WRA 2020b).

3. RESULTS AND DISCUSSION

3.1. Model calibration

Typhoons Fanapi, Talim, Megi, and Nesat were selected for model calibration, as field data were available. The total simulated field time was 43, 76, 72, and 46 h, respectively. The calibrated model results were simulated and compared with the field data in Figure 3. The root-mean-squared error and mean absolute error values were 1,450 and 921 mg/L in the

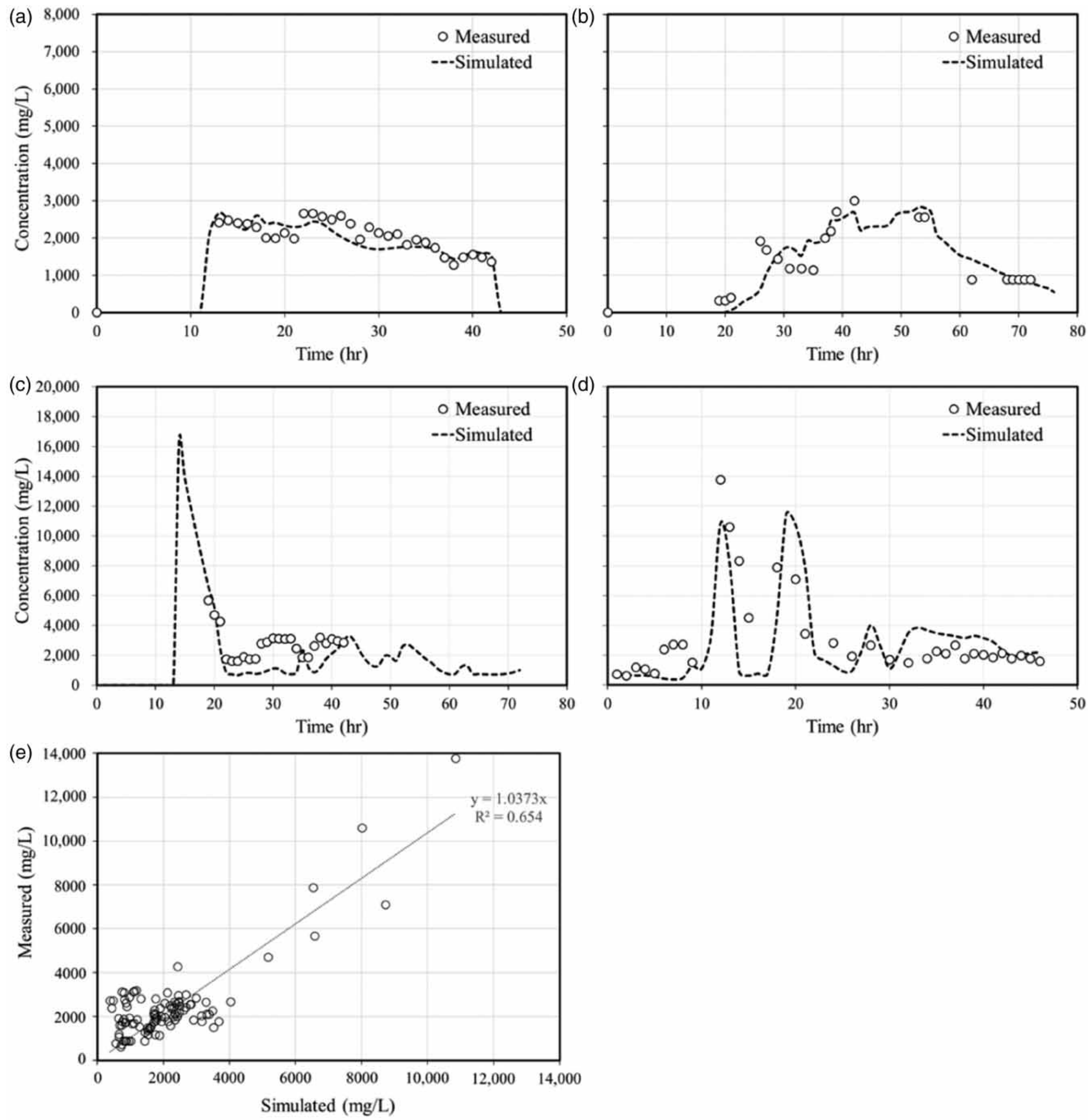

Figure 3 | Comparison of simulated and measured data of typhoons (a) Fanapi, (b) Talim, (c) Megi, and (d) Nesat. (e) Correlation performance.

comparison between simulated and measured data, respectively. The calibrated process led us to establish the model run procedure and identify key model parameters, as mentioned in Wang *et al.* (2020) and Huang *et al.* (2019), that are satisfied for this study application.

Based on four calibration cases, the correlation value between the simulation and measurement is drawn in Figure 3(e). The correlation value is about 0.654. Although the correlation value is not satisfactory, the tendency and values of simulated results also provide a reference and convincing value for this study.

3.2. Hydraulic and sediment transport simulation

For the simulation results of the hydraulic pattern and sediment transport in Table 3, the results of four topographic terrain conditions (Case 1, Case 2, Case 3, and Case 4) are discussed in this section.

First, the 2D simulation in this study depicts the peak inflow with the return period of the Q1.11 flow scenario. The flow velocity at the time of peak inflow with an initial water level of Elevation (EL.) 28 m, sediment concentration, and shear stress distribution are shown in Figure 4. From Figure 4, it can be observed that in the scenario without steel sheet piles (Case 1), the inflow turbid flow from the Zhuoshui River easily diffuses and spreads to the northern part of the reservoir area, with significant sediment accumulation in certain areas.

In the scenario with north steel sheet piles (Case 2-1), the inflow turbid flow from the Zhuoshui River is effectively concentrated within the flushing channel area, but there is still some sediment transport to the southern side of the flushing channel area. However, the sediment accumulation distribution on the north side of the flushing channel area improves compared to Case 1-1. In the scenario with additional steel sheet piles on the south side of the flushing channel area (Case 3-1 and Case 4-1), steel sheet piles with an elevation of EL. 32 m on the south side can concentrate the turbid flow within the flushing channel area toward the dam. However, there is still some turbid water overflow from the southern side of the EL. 30 m steel sheet

Table 3 | Simulated results of outflow items and desilting efficiency

Cases	Total inflow sediment yield (ton)	Total outflow sediment yield (ton)	Max. outflow concentration (mg/L)	Desilting efficiency (=total outflow sediment yield/total inflow sediment yield) of the spill shaft (%)	Variation of desilting efficiency (%)
Case1-1	27.46	17.31	11,779	63.04	–
Case1-2	27.46	17.11	11,769	62.31	–
Case1-3	165.19	107.28	19,847	64.94	–
Case1-4	539.75	360.9	20,300	66.86	–
Case2-1	27.46	21.18	21,823	77.13	14.09
Case2-2	27.46	20.41	21,052	74.33	12.02
Case2-3	165.19	117.29	22,525	71.00	6.06
Case2-4	539.75	370.43	22,550	68.63	1.77
Case3-1	27.46	22.15	22,267	80.66	17.63
Case3-2	27.46	21.87	21,663	79.64	17.33
Case3-3	165.19	125.23	22,652	75.81	10.87
Case3-4	539.75	389.34	23,204	72.13	5.27
Case3-5	68.57	53.94	22,408	78.66	–
Case3-6	129.98	99.86	22,535	76.83	–
Case3-7	226.33	168.61	22,736	74.50	–
Case3-8	276.28	203.65	22,822	73.71	–
Case3-9	388.59	281.72	23,000	72.50	–
Case4-1	27.46	22.73	26,229	82.80	19.76
Case4-2	27.46	22.45	25,517	81.75	19.44
Case4-3	165.19	128.94	26,389	78.06	13.11
Case4-4	539.75	394.34	29,333	73.06	6.20

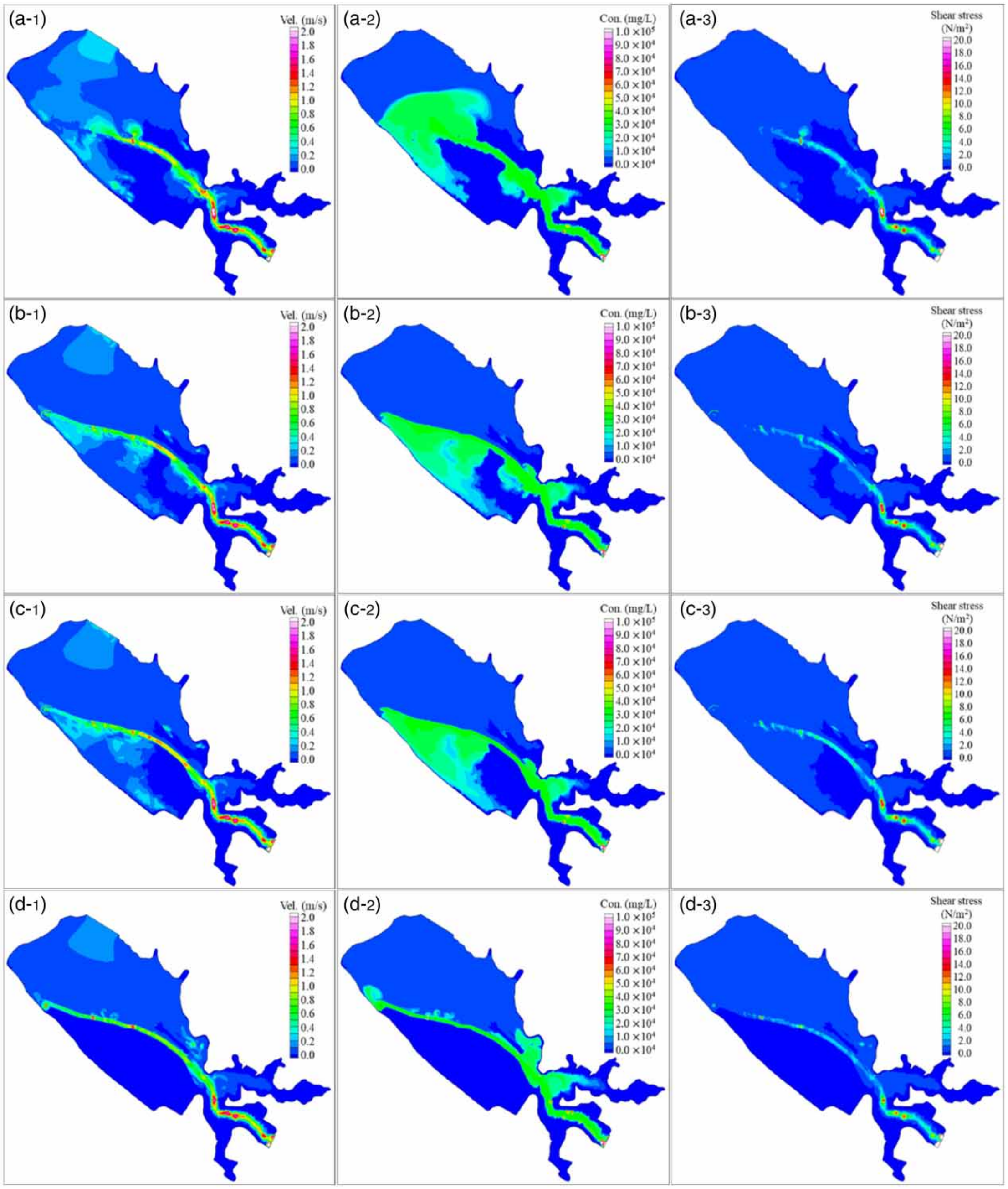

Figure 4 | Simulated velocity, concentration, and shear stress distribution of initial water level of 28 m under the Q1.11 flow scenario at peak inflow discharge. (a) Case 1, (b) Case 2, (c) Case 3, and (d) Case 4.

piles in Case 3-1 to the southern part of the reservoir area. The sediment accumulation distribution on the southern side of the segment shows improvement compared to Case 2-1.

The simulation results of a return period of the Q10 flow scenario and an initial water level of EL. 28 m for the Agongdian Reservoir are shown in Figure 5. From Figure 5, it can be observed that in the scenario without artificial guiding structures and with an increased flow, the turbid flow from the Zhuoshui River is influenced by the influx from the Wanglai River. As a result, the inflow turbid water is concentrated in the middle part of the reservoir area and is less prone to be transported to the spill shaft as in the Q1.11 flow scenario. Significant sediment accumulation occurs in most areas of the reservoir. In the scenario with a flushing channel and north steel sheet piles (Case 2-3), most of the inflow turbid flow from the Zhuoshui River is

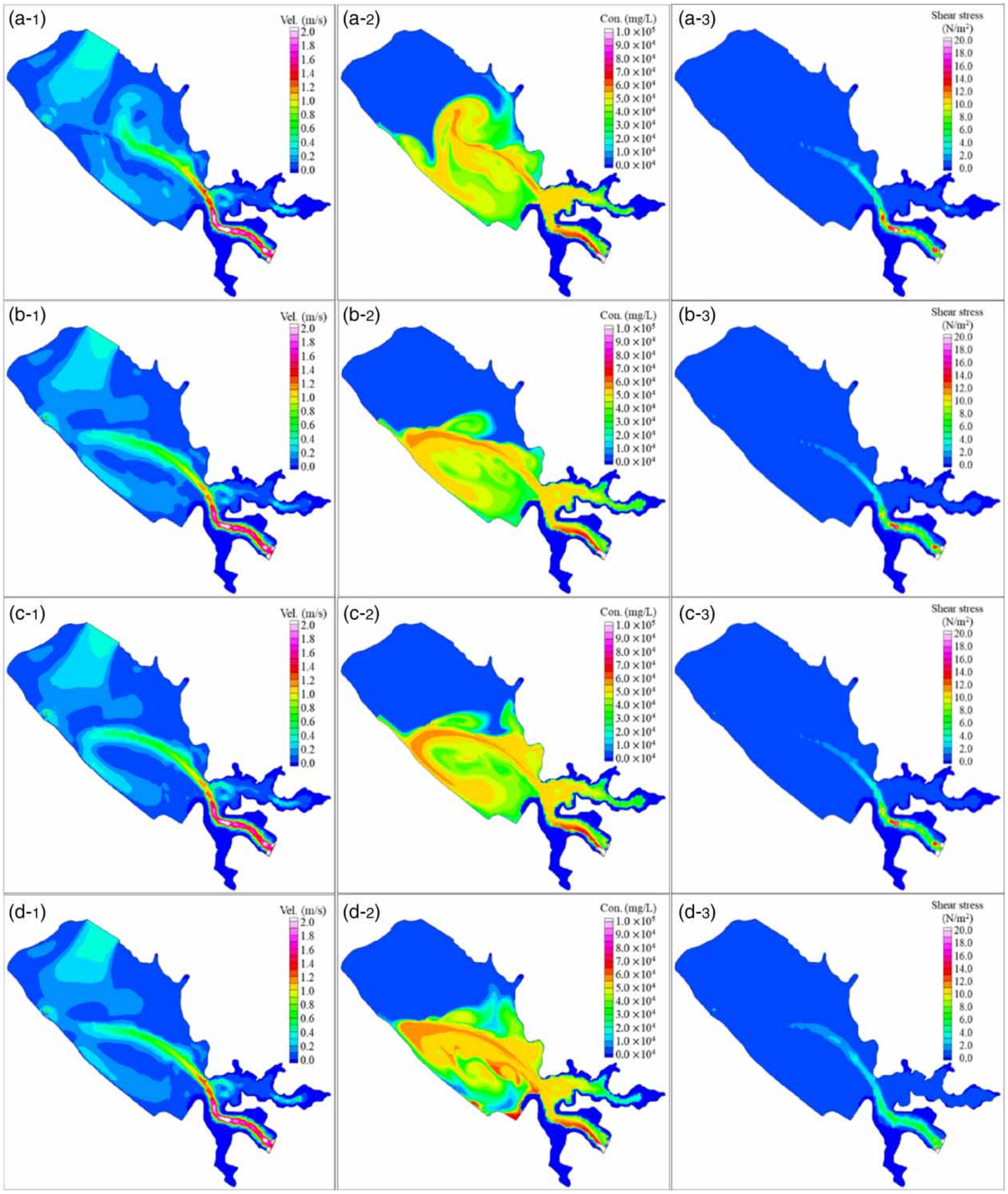

Figure 5 | Simulated velocity, concentration, and shear stress distribution of initial water level of 28 m under the Q10 flow scenario at peak inflow discharge. (a) Case 1, (b) Case 2, (c) Case 3, and (d) Case 4.

effectively concentrated within the flushing channel area. Some turbid water flows into the southern part of the reservoir area, resulting in noticeable conditions. Sediment accumulation occurs on both the north and south sides of the flushing channel, but the sediment accumulation on the north side is less than in Case 1-3. In the scenario with additional steel sheet piles on the south side of the flushing channel (Case 3-3 and Case 4-3), the flow conditions on the south side of the reservoir upstream part are similar to Case 2-3. However, some of the turbid water that flows through the southern EL. 30 m steel sheet piles to the spill shaft in Case 3-3 will overflow to the southern part of the reservoir, and the overall sediment accumulation in the reservoir downstream area is similar to Case 3-1.

Finally, a return period of the Q1000 flow scenario and an initial water level of EL. 28 m for the Agongdian Reservoir is simulated, as shown in Figure 6. From Figure 6, it can be observed that in the scenario without artificial guiding structures and with increased flow (Case 3-4 and Case 4-4) compared to Case 3-2 (Case 4-2) and Case 3-1 (Case 4-1), the turbid flow from the Zhuoshui River is influenced by the influx from the Wanglai Stream, yielding similar results to Case 1 and Case 2. The increased inflow discharge causes the inflow turbid water to tend toward the right bank in the middle and lower reaches of the reservoir, leading to turbulent flow within the reservoir and significant sediment accumulation in most areas of the reservoir. The extent and height of sediment accumulation increase compared to the Q10 flow scenario. In the scenario with north steel sheet piles, the inflow turbid water is more concentrated in the middle and upper reaches of the reservoir,

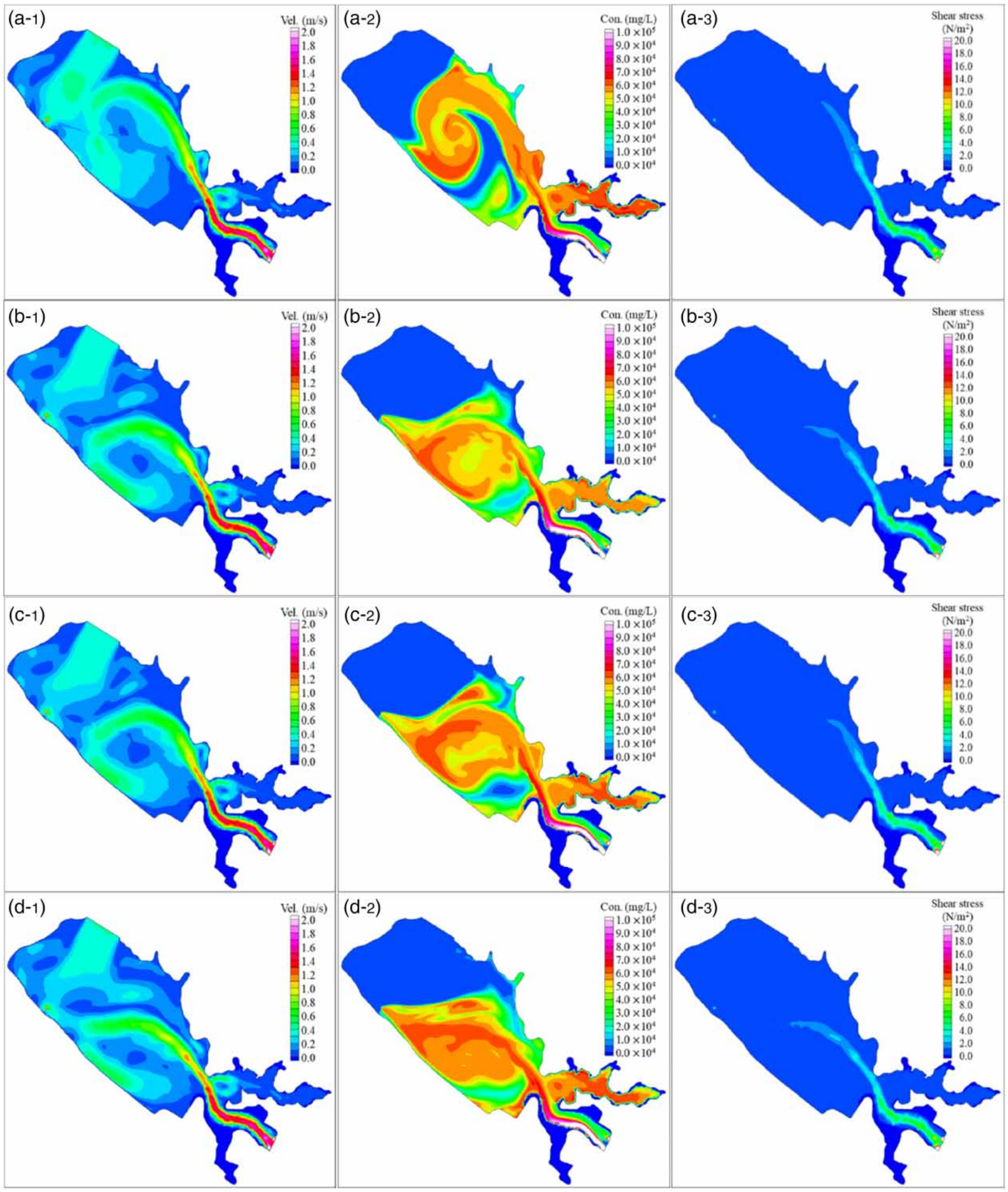

Figure 6 | Simulated velocity, concentration, and shear stress distribution of initial water level of 28 m under the Q1000 flow scenario at peak inflow discharge. (a) Case 1, (b) Case 2, (c) Case 3, and (d) Case 4.

with some turbid water overflowing to the northern and some turbid water flowing back to the southern part of the reservoir. The sediment accumulation on the north side of the flushing channel is less than in Case 1-4, but there is an increase in sediment accumulation on the south side. In the scenario with additional steel sheet piles on the south side of the flushing channel (Case 3-4 and Case 4-4), the flow conditions are similar to Case 3-3 and Case 4-3, but the concentration near the spill shaft is higher. The sediment accumulation on the south side of the flushing channel improves compared to Case 2-4 but only in the segment at the upper part of the south steel sheet piles. Overall, in the Q1000 flow scenario, the sediment concentration of the spill shaft is slightly higher than in the Q10 flow scenario. It can partially improve sediment accumulation in certain areas of the reservoir, but the effectiveness is also limited.

3.3. Outflow performance and desilting efficiency

In this study, the 2D numerical model at the Agongdian Reservoir was used to control the flow rates, sediment transport, and concentration variations at the inflow and outflow boundaries. The cumulative inflow and outflow sediment volumes, maximum outflow sediment concentrations, and sediment desilting efficiencies for various simulated scenarios were summarized, as presented in Table 3. From the sediment desilting efficiency ratios calculated in Table 3, it can be observed that under different scenarios of water levels, the sediment desilting efficiency at the lower water level (EL. 28 m) is slightly better than that at the higher water level (EL. 30 m), with increases in maximum outflow concentration and accumulated outflow sediment yield but with shorter transportation time. Under different inflow rate scenarios (Q1.11, Q10, Q1000), the accumulated outflow sediment yield and maximum outflow concentration are directly proportional to the flow rate. However, the desilting efficiency has a different trend between the basic topographic condition (Case 1) and the improvement conditions (Case 2 and Case 3). It reveals that the desilting efficiency values decrease with the inflow rate in Case 2 and Case 3 compared to Case 1. However, the artificial guiding structures have a negative effect on desilting efficiency under the same topographic condition (Case 2 or Case 3), even though the desilting efficiency values are both higher than in Case 1.

Under three topographical conditions, the desilting efficiency in Case 3 is larger than in Case 2, and Case 1 has a minimum value. When the initial water level is 28 m under the Q1.11 flow scenario, the desilting efficiency decreases by 14.09% (Case 2-1) and 17.63% (Case 3-1) scenario. When the initial water level is 30 m under the Q1.11 flow scenario, the desilting efficiency increases by 12.02% (Case 2-2) and 17.33% (Case 3-2). However, the values of desilting efficiency decrease with inflow rate in Case 2 and Case 3 at the same topographical condition. If both sides of the flushing channel have artificial guiding structures (Case 3), the desilting efficiency increases by 3.54, 4.81, and 3.50% compared to the case where only one side has artificial guiding structures (Case 2) when the initial water level is 28 m. When the initial water level is 30 m, the desilting efficiency increases by 5.31% (difference between Case 3-2 and Case 2-2), and the value is slightly larger than the initial water level in the 28 m condition (difference between Case 3-1 and Case 2-1). However, the desilting efficiency in Case 3 is superior to that in Case 2 under three flow conditions (Q1.11, Q10, Q1000).

If practical considerations are negligible, we investigate the desilting efficacy of a uniform-height steel shaft between the north and south in Case 3 and Case 4. The results, presented in Table 3 under Q1.11, Q10, and Q1000 scenarios, demonstrate a consistent increase in simulated desilting efficiency. The enhanced desilting efficacy (Case 3 compared to Case 4) ranges between 2.25 and 0.93%. These findings suggest that a fully uniform-height steel shaft in the flushing channel between the north and south can significantly improve desilting efficiency. However, practical engineering constraints in Case 4 limit its implementation, with increased desilting efficiency restricted, especially during extreme events. Therefore, we recommend deploying Case 3 as a valuable and feasible option for engineering applications.

Based on desilting efficiency simulation between normal and extreme events with artificial guiding structures (Case 3), the trend of desilting efficiency shows a slowdown slope performance, as shown in Figure 7. It reveals that the benefit of desilting efficiency decreases when inflow discharge increases. The slope change of the linear regression formula shows a 10 times difference between normal and extreme events. In addition, the lower bond of desilting efficiency of extreme events seems to have a 72.13% value, and the value is higher than the current condition of 66.86%. It has a 5.27% increasing value of desilting efficiency in extreme hydrological conditions. The higher performance of desilting efficiency happens in normal hydrological conditions, and it has a 17.63% increasing value.

4. CONCLUSIONS

Based on the simulated results of three topographical conditions, the desilting efficiency increases when artificial guiding structures of steel sheet piles are created. The increased desilting efficiency ranges from 17.63 to 1.77% in different flow

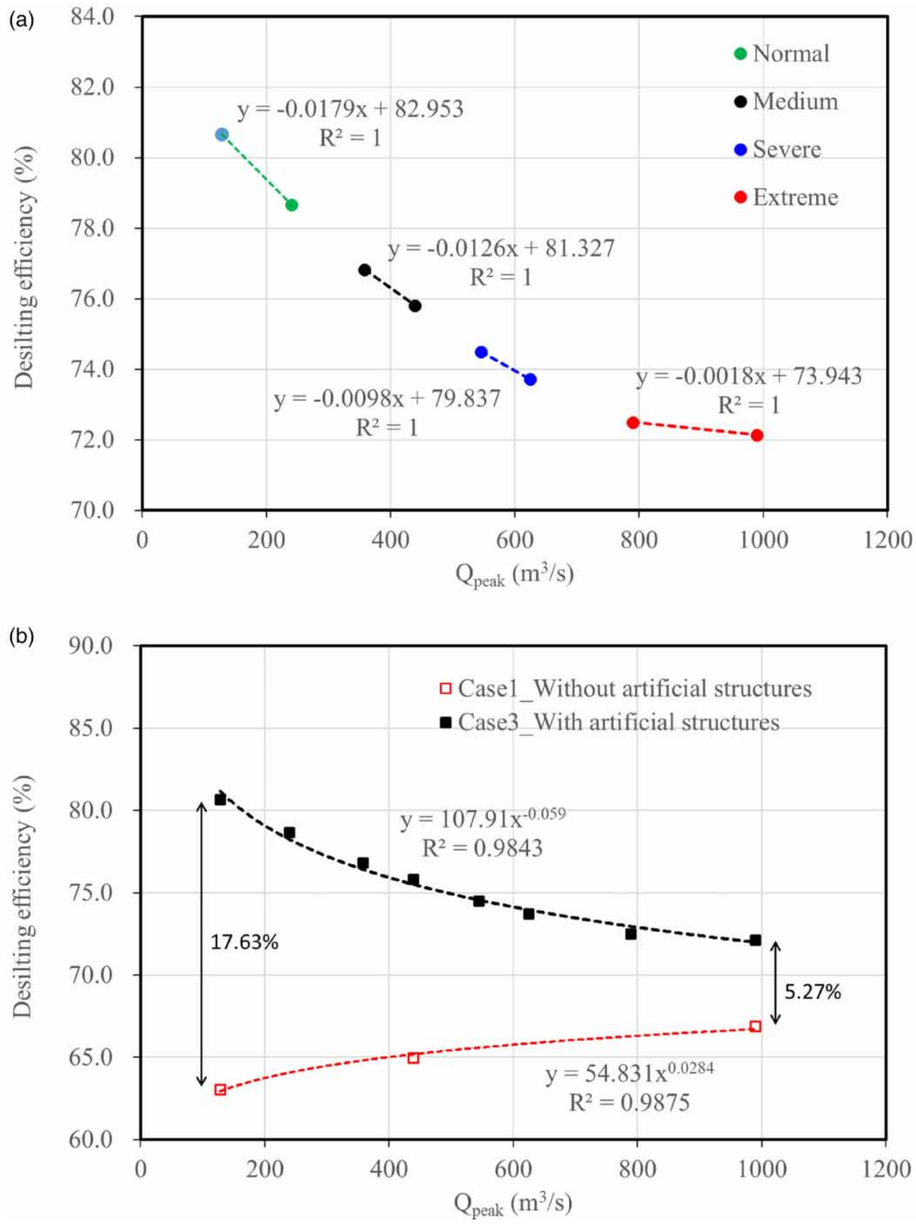

Figure 7 | Trend of desilting efficiency. (a) Distinguished trend of normal, medium, severe, and extreme in Case 3. (b) Comparison between normal and extreme events of Case 1 and Case 3.

scenarios. Not only the sediment concentration can be concentrated inside the flushing channel, but also the sediment transportation speeds up. The arrival time of inflow turbid water is earlier due to the constriction of the flushing channel. However, the significant desilting efficiency benefit occurs in the Q1.11 flow rather than in the Q10 and Q1000 flow scenarios due to the capacity of the flushing channel and outlet. When the inflow discharge is larger than the capacity of the flushing channel, the inflow turbid flow will overflow to the ambient reservoir area and decrease the desilting efficiency of the spill shaft. In addition, the steel sheet piles will constrain the flow field, resulting in decreased consequence of desilting efficiency as the hydrological conditions become more extreme. Even though there is a negative effect, the steel sheet piles created on both sides of the flushing channel can help improve desilting efficiency and are valuable to sediment management. Based on the simulation results, the lower bond of desilting efficiency is 72.13% during extreme events. In addition, applying artificial countermeasures to enhance desilting efficiency yields an increasing value from 5.27% during extreme hydrological events to 17.63% during normal hydrological events.

However, this study represents only interim results at the current stage. There are still shortcomings in this study or areas that warrant further investigation. We present three potential suggestions for future work: the first involves the variation in the geometry of the flushing channel, the second concerns the deployment of steel shafts, and the third relates to the operational uncertainty of reservoir desilting sequences. We believe that these relevant studies could be more beneficial and serve as references for reservoir sediment management.

ACKNOWLEDGEMENTS

The authors acknowledge the Southern Region Water Resources Branch, Taiwan, and Liming Engineering Consultants Co., Ltd, Taiwan, for providing the essential data for analyses and simulations. The authors also acknowledge the National Taiwan University for manpower and technique support.

AUTHOR CONTRIBUTIONS

F-ZL developed the principal concepts, generated the analyzed data, and wrote the manuscript. NLHN edited the manuscript.

DATA AVAILABILITY STATEMENT

All relevant data are included in the paper or its Supplementary Information.

CONFLICT OF INTEREST

The authors declare there is no conflict.

REFERENCES

Albayrak, I., Müller-Hagmann, M. & Boes, R. 2019 Efficiency evaluation of Swiss Sediment Bypass Tunnels. In: *Proceedings of the 3rd International Workshop on Sediment Bypass Tunnels* National Taiwan University, Taipei, pp. 239–245.

Anari, R., Hotchkiss, R. H. & Langendoen, E. J. 2020 Elements for the successful computer simulation of sediment management strategies for reservoirs. *Water* **12** (3), 714.

Annandale, G. W., Morris, G. L. & Karki, P. 2016 *Extending the Life of Reservoirs*. World Bank, Washington, DC.

Baghalian, S. & Ghodsian, M. 2020 Experimental study on the effects of artificial bed roughness on turbidity currents over abrupt bed slope change. *International Journal of Sediment Research* **35** (3), 256–268.

Boes, R., Müller-Hagmann, M. & Albayrak, I. 2019 Design, operation and morphological effects of bypass tunnels as a sediment routing technique. In: *Proceedings of the 3rd International Workshop on Sediment Bypass Tunnels.* National Taiwan University, Taipei, pp. 40–50.

Chen, S. Y. 2020 *Applying the two-Dimensional (2D) Layer-Averaged Turbidity Current Model to Estimate Outlet Sediment Concentration and Desilting Efficiency in the Zengwen Reservoir*. Master's Thesis, National Taiwan University.

Chen, P. A. 2022 *Integration of Multiple Outlets' Operation and Sediment Management Options in the Reservoir for Increasing Efficiency of Turbidity Current Venting and Clear Water Storages*. Doctoral Dissertation, Kyoto University.

Chen, C. N. & Tsai, C. H. 2017 Estimating sediment flushing efficiency of a shaft spillway pipe and bed evolution in a reservoir. *Water* **9** (12), 924.

De Cesare, G., Boillat, J. L. & Schleiss, A. J. 2006 Circulation in stratified lakes due to flood-induced turbidity currents. *Journal of Environmental Engineering* **132** (11), 1508–1517.

Ge, H., Zhu, L., Lin, Q. & Deng, C. 2021 Analysis of sediment deposition in Lushui Reservoir to guide dredging. *Arabian Journal of Geosciences* **14** (2), Article 2.

Hu, P., Cao, Z., Pender, G. & Tan, G. 2012 Numerical modelling of turbidity currents in the Xiaolangdi reservoir, Yellow River, China. *Journal of Hydrology* **464**, 41–53.

Huang, C. C., Lai, Y. G., Lai, J. S. & Tan, Y. C. 2019 Field and numerical modeling study of turbidity current in Shimen Reservoir during typhoon events. *Journal of Hydraulic Engineering* **145** (5), 05019003.

Hung, C. C., Lai, J. S. & Huang, C. C. 2022 An efficient and economic desilitation strategy for reservoir sustainable development under the threat of extreme flooding threaten. *Journal of Water and Climate Change* **13** (3), 1257–1274.

Kantoush, S. A., Mousa, A., Shahmirzadi, E. M., Toshiyuki, T. & Sumi, T. 2021 Pilot field implementation of suction dredging for sustainable sediment management of dam reservoirs. *Journal of Hydraulic Engineering* **147** (2), Article 2.

Kondolf, G. M., Gao, Y., Annandale, G. W., Morris, G. L., Jiang, E., Zhang, J., Cao, Y., Carling, P., Fu, K. & Guo, Q. 2014 Sustainable sediment management in reservoirs and regulated rivers: Experiences from five continents. *Earth's Future* **2** (5), 256–280.

Lai, Y. G. 2010 Two-dimensional depth-averaged flow modeling with an unstructured hybrid mesh. *Journal of Hydraulic Engineering* **136** (1), 12–23.

Lai, Y. G. 2020 A two-dimensional depth-averaged sediment transport mobile-bed model with polygonal meshes. *Water* **12** (4), 1032.
Lai, J. S. & Shen, H. W. 1996 Flushing sediment through reservoirs. *Journal of Hydraulic Research* **34**, 237–255.
Lee, F. Z., Huang, M. S., Liu, C. C., Song, D. R., Liu, R. & Chiueh, P. T. 2021 Application of 2-D numerical model on flood control and sediment transportation for barrage types. *Journal of Taiwan Agricultural Engineering* **67** (2), 32–43.
Lee, F. Z., Liu, C. C., Lai, J. S. & Chiueh, P. T. 2023a Study on the application of flushing channel with guide wall to reduce sedimentation in a reservoir. *Journal of Taiwan Agricultural Engineering* **69** (2), 11–21.
Lee, F. Z., Chen, S. Y., Lai, J. S., Tan, Y. C. & Yu, H. L. 2023b Apply two-dimensional layer-averaged model and theoretical orifice flow equations to estimate desilting efficiency. *Taiwan Water Conservancy* **71** (1), 39–50.
Morris, G. L. 2020 Classification of management alternatives to combat reservoir sedimentation. *Water* **12**, 3.
Morris, J. & Fan, G. L. 2010 *Reservoir Sedimentation Handbook*. McGraw-Hill, New York.
Oehy, C. D. & Schleiss, A. J. 2007 Control of turbidity currents in reservoirs by solid and permeable obstacles. *Journal of Hydraulic Engineering* **133** (6), 637–648.
Parker, G. 1990 Surface-based bedload transport relation for gravel rivers. *Journal of Hydraulic Research* **28** (4), 417–436.
Samad, N., Chauhdry, M. H., Ashraf, M., Saleem, M., Hamid, Q., Babar, U., Tariq, H. & Farid, M. S. 2016 Sediment yield assessment and identification of check dam sites for Rawal Dam catchment. *Arabian Journal of Geosciences* **9** (6), Article 6.
Smith, C., Williams, J., Nejadhashemi, A. P., Woznicki, S. & Leatherman, J. 2013 Cropland management versus dredging: An economic analysis of reservoir sediment management. *Lake and Reservoir Management* **29** (3), Article 3.
Wang, H. W., Tsai, B. S., Hwang, C., Chen, G. W. & Kuo, W. C. 2020 Efficiency of the drawdown flushing and partition desilting of a reservoir in Taiwan. *Water* **12** (8), 2166.
Wieland, M. 2010 Life-span of storage dams. *International Water Power & Dam Construction* **2010**, 32–35.
Wisser, D., Frolking, S., Hagen, S. & Bierkens, M. F. 2013 Beyond peak reservoir storage? A global estimate of declining water storage capacity in large reservoirs. *Water Resources Research* **49** (9), 5732–5739.
WRA 2015 *Sediment Observation and Efficiency Evaluation for Desiltation of Agongdian Reservoir by Using Empty Flushing in* 2015. Tainan, Taiwan.
WRA 2020a *Reservoir Desiltation, Technology and Management*. Taipei, Taiwan.
WRA 2020b *Sediment Observation for Desiltation of Agongdian Reservoir by Using Empty Flushing and Consultation for Flood Control Operation in* 2020. Tainan, Taiwan.
WRA 2022a *Measure Program about the Sedimentation Survey for Agongdian Reservoir and Agongdian River in* 2022. Tainan, Taiwan.
WRA 2022b *The Research Project of Agongdian Reservoir Dredging Strategies Review and Water Resources Utilization Improvement*. Tainan, Taiwan.
WRA 2003 *Hydraulic Model Studies on the Functions and Operations of Silting Prevention in Agongdian Reservoir – Final Report*. Taichung, Taiwan.
Zeng, Y., Meng, X., Zhang, Y., Dai, W., Fang, N. & Shi, Z. 2022 Estimation of the volume of sediment deposited behind check dams based on UAV remote sensing. *Journal of Hydrology* **612**, 128143.
Zulfan, J., Ginting, B. M. & Rimawan, R. 2023 Assessment of reservoir sedimentation and mitigation measures using 2D hydrodynamic modeling: Case study of Pandanduri Reservoir, Indonesia. *IOP Conference Series: Earth and Environmental Science* **1135** (1), Article 1.

First received 25 October 2023; accepted in revised form 30 March 2024. Available online 3 June 2024